Splitting of the peak of electromagnetically induced transparency by the higher-order spatial harmonics of the atomic coherence

S. A. Babin, D. V. Churkin, E. V. Podivilov, V. V. Potapov, and D. A. Shapiro
Institute of Automation and Electrometry, Siberian Branch, Russian Academy of Sciences, Novosibirsk 630090, Russia
(Received 16 August 2002; published 11 April 2003)

The interaction of a two-level system with a strong standing wave is examined by the probe field resonant to the adjacent transition in the Λ configuration of Ar II. The known peak of electromagnetically induced transparency is observed in the absorption spectrum at the detuning of the probe field proportional to the detuning of the strong field. Along with it, the different structure has been found at the line center, independently of the strong-field frequency. The calculations clarify that the central structure is induced by the higher-order spatial harmonics of the atomic coherence induced at the probe transition. The effect results in steep frequency dependence of the refractive index at the line center.

DOI: 10.1103/PhysRevA.67.043808 PACS number(s): 42.50.Gy, 42.50.Hz, 42.62.Fi

It is well known that absorption of light in an atomic medium at resonant frequency may be reduced or even eliminated by application of a strong ''drive'' laser field to an adjacent transition. This phenomenon called electromagnetically induced transparency (EIT), see Refs. [1,2], underlies a variety of effects driven by atomic coherence and interference, such as resonant enhancement of nonlinear optical processes [3], amplification and lasing without inversion [4], and inhibition of two-photon absorption [5]. In addition to coherently-driven changes of the absorption coefficient, the EIT resonance has specific dispersive features (steep positive dispersion inside a transparency window) that have been recently applied for slowing down and even ''stopping'' or ''storage'' of the light [6–8] that could have important applications in quantum computing. For these applications, the aim is to obtain narrower EIT resonance and as a result steeper dispersion, but relaxation, collisional, power and Doppler broadening significantly worsen the shape of the EIT resonance [9]. To diminish their role and obtain the desired dispersion slope characteristic, various techniques such as cooled atomic gas [6], multiple drive fields in a multilevel system [10] or solid-state medium [8] are used.

Let us mention that the EIT experimental techniques are usually based on running ''drive'' and ''probe'' waves. In this paper, we treat the EIT in a basic Λ-system but with standing-wave drive. In this case, the driving field is modulated in space and as a result qualitatively different effects may be induced by spatial harmonics of atomic coherence. It is predicted and experimentally proved that different resonant structure inside the transparency window appears at specific conditions. At zero drive detuning, the effect looks like ''splitting'' of the usual EIT resonance in probe-field spectrum. It is shown that the additional resonance is attributed to interaction of light with slow atoms and insensitive to the Doppler broadening and as a result occurs narrow. Thus it may be treated as a different approach to produce steep dispersion (positive or negative) inside the transparency window applicable to atomic systems in light-stopping experiments as well as in other EIT-related effects.

Basic nonlinear spectroscopic effects of a strong standing wave have been studied in the 1960s and 1970s. Calculation of spontaneous emission spectra in a two-level system [11] and the Lamb dip [12] reveals oscillations of level populations, those were interpreted [13] as multiphoton Bennett structures. In the three-level system, the oscillations manifest itself in probe-field spectrum at the adjacent transition, as had been shown by Feldman and Feld [14]. Recently, three-level systems with a standing wave were studied in connection with optically pumped infrared molecular lasers [15] and up-conversion in ladder scheme [16]. The effect of cavity under EIT conditions is also treated in view of photon-photon interactions, see, for example, Ref. [17], or EIT-window narrowing due to cooperative effects [18], but neither paper considers standing-wave drive.

We explore the Λ scheme of Ar II shown in Fig. 1. The starting, intermediate, and final levels of the Raman scheme were $|n\rangle = 4s\,^2P_{1/2}$, $|m\rangle = 4p\,^2S_{1/2}$, and $|l\rangle = 3s\,^2P_{3/2}$, respectively. The Λ system under study has the following relaxation rates $\Gamma_n = 300, \Gamma_m = 15, \Gamma_l = 8$, and Einstein coefficients $A_{mn} = 9$, $A_{ml} = 1$ (in units of $10^7\ \mathrm{s}^{-1}$). The populations of levels in plasma are $N_n \sim 1, N_m \sim 5$, and $N_l \sim 100$ (in units of $10^9\ \mathrm{cm}^{-3}$). The pump is a blue standing wave of wavelength $\lambda = 458$ nm, the probe is a red running wave of wavelength $\lambda_\mu = 648$ nm.

The experiment was based on the ionic anti-Stokes Raman laser device [19]. The setup modified for the Stokes wave is shown in Fig. 2. Discharge tube 1 was placed in the cavity formed by mirrors 2 and 3 of a high reflection coefficient for

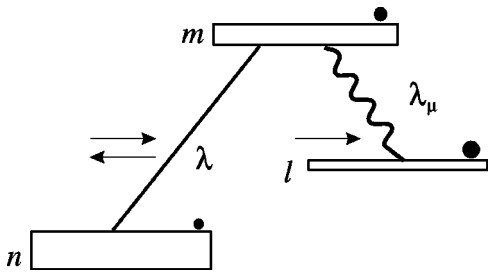

FIG. 1. Level diagram. Relative relaxation rates and populations of levels are shown schematically by the height of box and diameter of circle, $\Gamma_l < \Gamma_m \ll \Gamma_n$, $N_n < N_m \ll N_l$. The straight line denotes the strong standing-wave pump; the wavy line is the weak running probe.

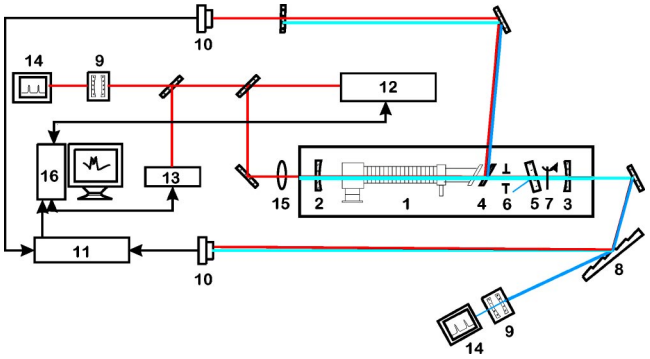

FIG. 2. Scheme of the experiment.

generated radiation and transparent for the probe wave. Thus two fields were present inside the cavity: standing blue wave and running red one, both with parallel linear polarizations. Etalon 5 provided the selection and tuning of the generation frequency. Diaphragm 6 selected TEM_{00} transverse mode. The cavity losses at $\lambda = 458$ nm were about 0.3%, then the high-intensity single-frequency operation was achieved. The blue drive and red probe beams were separated by diffraction grating 8. Spectra were analyzed by scanning Fabry-Perot interferometers 9 with oscilloscopes 14 and λ-meter 13. The laser beam was modulated by chopper 7. Photodiodes 10 produced signal and reference for synchronous detector 11. As a source of the probe field, tunable dye laser 12 was employed. Automatic scanning system [20] made it possible to vary the frequency continuously within 4.5 GHz range. The probe beam was focused by lens 15 into the middle of the tube and deflected by plate 4. The angle between the probe and generated beams was kept around 10^{-3} to avoid feedback. The synchronous detector subtracted the Doppler background from the probe-field spectrum. The frequency scanning and data acquisition were carried out by PC 16 with discrete step 20 MHz.

Figure 3 shows the probe-field spectra; upward direction corresponds to induced transparency, downward is absorption. Figure 3(a) shows the resonant case ($\Delta = 0$). The bottom curve demonstrates well-known ac Stark splitting of absorption spectrum with EIT peak between the split components. With increase in the intensity the transparency peak broadens and becomes split. The splitting is enhanced with intensity (top two curves). Small asymmetry is due to the "lens" effect [21] and can be compensated by a small detuning Δ. The maximum intensity (topmost curve) corresponds to the Rabi frequency for each of two running components $\Omega = 100$ MHz. Figure 3(b) describes the Δ-dependence at $\Omega = 100$ MHz. At pump detuning $\Delta > 0.7$ GHz, the distinct additional peak is formed at the center, along with the main peak. The second peak is small, but resolvable up to detuning $\Delta \sim 2$ GHz. The central structure is by two times narrower than the main. In the topmost curve ($\Delta = 2$ GHz), the central peak has poor contrast. Note, that the flat dip at negative detuning corresponds to the Bennett hole induced by counter-propagating component.

The peak of EIT had been expected and observed at

$$\frac{\Delta_\mu}{k_\mu} = \frac{\Delta}{k}. \tag{1}$$

The condition means that the probe wave and the copropagating component of the standing wave interact with the same velocity group. Along with the expected peak, the additional structure was resolved in the line center. Its position $\Delta_\mu = 0$ was independent of the detuning Δ. We found no analog in the literature, then revised the perturbation theory. The structure is interpreted as effect of higher spatial harmonics of coherence. It is insensitive to the detuning Δ, since only atoms with zero velocity pay the contribution into the structure. The continued-fraction expansion, calculated numerically for higher pump intensity, yields similar results. Moreover, below we demonstrate that the additional central structure is a universal phenomenon arisen not only under specific experimental conditions.

The absorption spectrum is given by the off-diagonal element of the density matrix $\rho_{ml} = \rho_\mu \exp(ik_\mu x - i\omega_\mu t)$,

$$P_\mu(\Delta_\mu) = -2\hbar\omega_\mu \mathrm{Re}\langle i\Omega_\mu^* \rho_\mu \rangle, \tag{2}$$

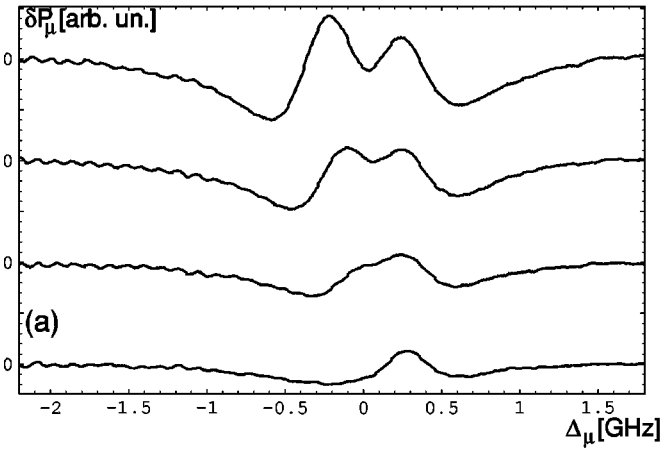

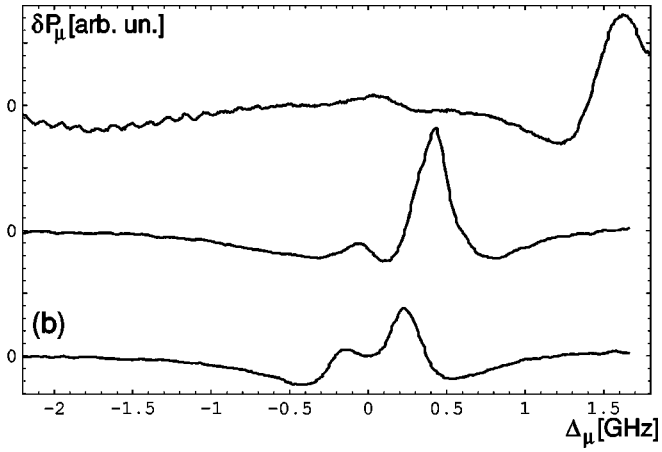

FIG. 3. Measured spectra. (a) At $\Delta = 0$ and different Rabi frequencies, from bottom to top: $\Omega = 0$, 50, 75, and 100 MHz. (b) At $\Omega = 100$ MHz and different detunings, from bottom to top: $\Delta =$ 0.2, 0.7, and 2 GHz. The amplitude of the last curve is doubled.

where the angular brackets denote averaging over velocity and coordinate, ω_μ, $\Omega_\mu=\vec{E}_\mu\cdot\vec{\mu}_{ml}/2\hbar$ are the frequency and Rabi frequency of probe wave $\vec{E}_\mu(x,t)=\vec{E}_\mu\exp(ik_\mu x - i\omega_\mu t)$, and μ_{ml} is the dipole moment. The off-diagonal element determines the coherence between levels.

The high relative population of final level l in experiment allows one to ignore all effects induced by the strong standing wave related to changes in both populations and coherence at the working transition. The main nonlinear spectroscopic effect in such a system is related to mixing of off-diagonal elements ρ_{ml},ρ_{nl} on both test and forbidden transitions by the standing-wave field. To emphasize the effect, we set $N_m=N_n=0$ reducing the density-matrix equations to a pair of equations for off-diagonal elements at probe ρ_μ transition and two-photon transition $\rho_{ln}=\rho_\nu\exp[-ik_\mu x - i(\omega-\omega_\mu)t]$:

$$[\Gamma_{ml}-i(\Delta_\mu-k_\mu v)+v\partial_x]\rho_\mu+i(\Omega_+e^{ikx}+\Omega_-e^{-ikx})\rho_\nu^* = i\Omega_\mu N_l(v), \tag{3}$$

$$[\Gamma_{nl}+i(\Delta-\Delta_\mu+k_\mu v)+v\partial_x]\rho_\nu^*+i(\Omega_+^*e^{-ikx}+\Omega_-^*e^{ikx})\rho_\mu = 0.$$

Here Γ_{ml},Γ_{nl} are the relaxation constants, ∂_x denotes the derivative operator with respect to x, $\vec{E}(x,t)=2\vec{E}\cos kx\exp(-i\omega t)$ is the standing wave, $\Omega=\vec{E}\cdot\vec{\mu}_{mn}/2\hbar$ is its Rabi frequency, μ_{mn} is the dipole moment,

$$N_l(v)=\frac{N_l\exp(-v^2/v_T^2)}{\sqrt{\pi}v_T} \tag{4}$$

is the Maxwellian distribution of the population N_l over velocities, and v_T is the thermal velocity. We denote two amplitudes as Ω_+ for its copropagating component and Ω_- for the counterpropagating one. If one express ρ_μ and ρ_ν as a Fourier series as a function of coordinate, i.e., spatial harmonics,

$$\rho_\mu=\sum_{n=-\infty}^{\infty}\rho_\mu^{(n)}e^{2nikx},\quad \rho_\nu^*=\sum_{n=-\infty}^{\infty}\rho_\nu^{(n)*}e^{(2n-1)ikx}, \tag{5}$$

the set (3) reduces to difference equations that relate amplitudes of spatial harmonics with neighbor numbers: $\rho_\nu^{(n)*}$ to $\rho_\mu^{(n)}$ and $\rho_\mu^{(n-1)}$ [22]. At $\Omega_+=\Omega_-=\Omega=0$ Eqs. (3) are decoupled and only the lowest harmonics $n=0$ enters the result. At small $\Omega\ll\Gamma,\Delta$ the coefficients $\rho_{\mu,\nu}^{(n)}$ harmonics at $n=\pm1,\pm2$ are small and can be found within the perturbation theory. At strong field $\Omega\gg\Gamma,\Delta$ the perturbation theory is not valid. The solution of difference equations can be written as a continued fraction.

For this reason, the main tool of study is numerical calculations. However, at small fields, the problem can be analyzed using perturbation theory. The main goal of such an analysis is to demonstrate that the central resonances in probe-field spectrum being caused by the higher spatial harmonics of the coherence. Importantly, that in the first order of the perturbation theory, the higher spatial harmonics do not contribute to the spectrum after the averaging over velocities in the Doppler limit ($kv_T\gg\Gamma$). In the Stokes case ($k_\mu<k$), the first nonlinear correction describes the EIT peak of the width

$$\Gamma_p=\frac{k_\mu}{k}\Gamma_{nl}+\frac{k-k_\mu}{k}\Gamma_{ml}, \tag{6}$$

at frequency $\Delta_\mu=k_\mu\Delta/k$,

$$\delta P_\mu^{(1)}=P_\mu(0)-P_\mu^{(1)}(\Omega) =2\hbar\omega_\mu|\Omega_\mu|^2\frac{\sqrt{\pi}}{kv_T}N_l\exp(-\Delta_\mu^2/k_\mu^2v_T^2) \times\mathrm{Re}\frac{2|\Omega_+|^2(k-k_\mu)}{k[\Gamma_p-i(\Delta_\mu-k_\mu\Delta/k)]^2}. \tag{7}$$

Therefore, the standing-wave effects appear in the second-order perturbation theory.

After accurate solving Eq. (3) to the terms of fourth order in $\Omega_\pm$ and integrating the result over velocities in the Doppler limit using the theory of residues, we obtain the following expression for the second-order correction to the spectrum:

$$\delta P_\mu^{(2)}=-2\hbar\omega_\mu|\Omega_\mu|^2\frac{\sqrt{\pi}N_l\exp(-\Delta_\mu^2/k_\mu^2v_T^2)}{kv_T} \times\mathrm{Re}\frac{2|\Omega_+|^2(k-k_\mu)/k}{\gamma_p^2}\left[\frac{3|\Omega_+|^2k_\mu(k-k_\mu)/k^2}{\gamma_p^2} +\frac{|\Omega_-|^2(k-k_\mu)^2/k^2}{2\gamma_p[\Gamma_{nl}-i(\Delta_\mu-\Delta)]}+\frac{|\Omega_-|^2k_\mu^2(2k-k_\mu)/k^3}{4(\Gamma_{ml}-i\Delta_\mu)^2} +\frac{|\Omega_-|^2k_\mu^2(k-k_\mu)/k^3}{\gamma_p(\Gamma_{ml}-i\Delta_\mu)}\right]. \tag{8}$$

Here $\gamma_p=[\Gamma_p-i(k\Delta_\mu-k_\mu\Delta)]/k$, the $\Omega=0$ background is subtracted: $P_\mu(\Omega)=P_\mu|_{\Omega=0}-\delta P_\mu^{(1)}-\delta P_\mu^{(2)}-\cdots$. The first term in square brackets describes the broadening of the EIT peak and increasing in its amplitude. The second term describes the contour similar to a two-photon resonance, it peaks at frequency $\Delta_\mu=\Delta$. The rest two terms are caused by the spatial modulation of coherence ρ_μ at the probe transition ml and result in the nonlinear structure at $\Delta_\mu=0$. This structure is distinguishable under relation $\Gamma_{ml}\ll\Gamma_{nl}$ corresponding to experimental conditions. The expression of this type was obtained earlier [23], but the opposite limiting case $\Gamma_{nl}\ll\Gamma_{ml}$ was analyzed.

Equation (8) is valid at low-pump intensity. The expression for the probe-field spectrum at arbitrary intensity of the standing wave [14] in the case of our interest, when only the final level is populated, can be written as $P_\mu=\mathrm{Im}R_\mu$, where

$$R_\mu\propto N_l|\Omega_\mu|^2\langle[L_0^{-1}-|\Omega|^2(u_++u_-)]^{-1}\rangle_v, \tag{9}$$

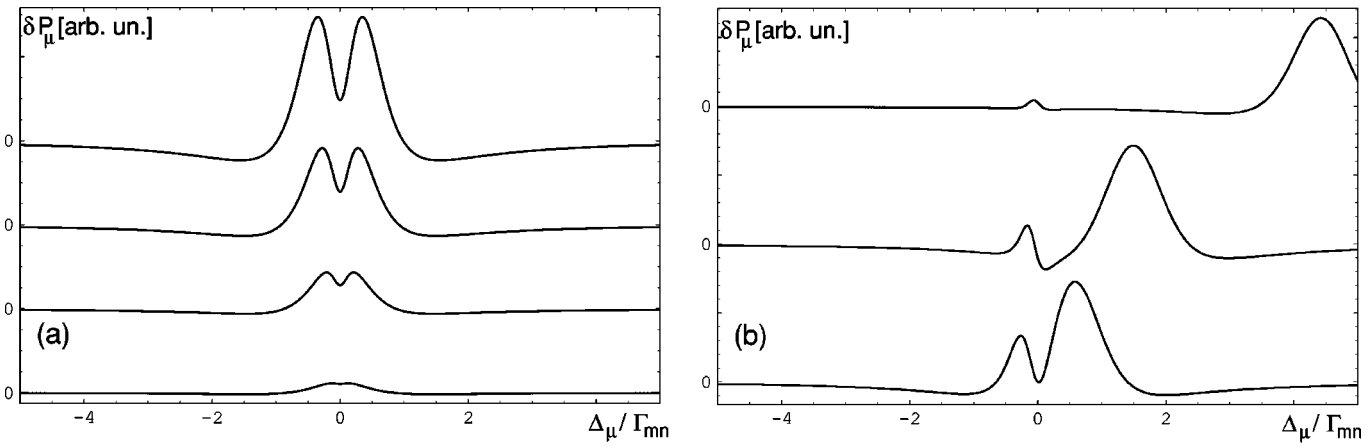

FIG. 4. Calculated spectra. (a) At $\Delta=0$, $kv_T=20\Gamma_{mn}$, $\Gamma_{ml}/\Gamma_{nl}=1/6$, $\Gamma_{mn}\approx\Gamma_{nl}$ and different Rabi frequencies, from bottom to top: $\Omega/\Gamma_{mn}=0.1$, 0.2, 0.3, and 0.4. (b) At $\Omega/\Gamma_{mn}=0.4$ and different detunings, from bottom to top: $\Delta/\Gamma_{mn}=$ 0.7, 2.2, and 6.6.

$$u_{\pm}=\cfrac{L_{\pm 1}}{1-\cfrac{|\Omega|^2 L_{\pm 1}L_{\pm 2}}{1-\cfrac{|\Omega|^2 L_{\pm 2}L_{\pm 3}}{1-\cfrac{|\Omega|^2 L_{\pm 3}L_{\pm 4}}{1-\ldots}}}}, \tag{10}$$

$$L_j^{-1}=\begin{cases}\varepsilon-(k_\mu+jk)v+i\Gamma_{nl}, & j=\pm 1,\pm 3,\ldots\\ \Delta_\mu-(k_\mu+jk)v+i\Gamma_{ml}, & j=0,\pm 2,\ldots.\end{cases}$$

Here $\langle\ldots\rangle_v$ means the average over velocity, $\varepsilon=\Delta_\mu-\Delta$. The continued fraction (10) is calculated and integrated with Maxwellian distribution numerically. Figure 4(a) shows the resonant case $\Delta=0$, while Fig. 4(b) illustrates the nonresonant case. Together with the main EIT peak shifted with the detuning, the additional structure arises in the center. Under resonance condition the structure is a dip; far from the resonance it transforms into a peak. Its behavior is in qualitative agreement with experiment, Fig. 3. The plots calculated from Eq. (8) practically coincide with those in Fig. 4 at low intensities, $\Omega/\Gamma_{mn}<0.4$ corresponding to experiment. Note, that the scale in the experimental plot $\Delta_\mu=1.5$ GHz corresponds to the dimensionless scale in the calculated one, $\Delta_\mu/\Gamma_{mn}=1.5\ \text{GHz}/0.3\ \text{GHz}=5$.

Thus, the comparison between the theory and experiment demonstrates similar dependence either on Ω, or Δ. In resonant case, the EIT peak broadens with Ω. At the same time, the dip in the center arises already at $\Omega/\Gamma_{mn}\sim 0.1$, its depth grows with Ω. The EIT peak is shifted synchronously with detuning Δ, since it is formed when strong and probe waves interact with the same velocity group of atoms. The resonance structure is motionless because it is formed by atoms with zero velocity. The spatial modulation of coherence is caused by the simultaneous action of both components of the standing wave. Then the effect of higher harmonics is maximal for slow atoms. Atoms in the nodal points of the standing wave are insensitive to the strong field, hence the EIT vanishes for these particles. At the same time, the EIT is maximal at the antinodes. After averaging along the tube and over velocities, the additional structure appears in the center of probe-field spectrum.

Let us note that the effect was missed in the classical paper by Feldman and Feld [14], because their calculations were performed at the condition $\Gamma_{ml}=\Gamma_{nl}$ when the effect at the exact resonance $\Delta=0$ is absent. In our case the ''slow atom'' dip of the width Γ_{ml} splits the EIT resonance of the width $\Gamma_p\simeq\Gamma_{nl}$ at the line center because $\Gamma_{ml}\ll\Gamma_{nl},\Gamma_{mn}$. Taking into account plasma collisions, we estimate this additional splitting as $\Gamma_{ml}\simeq 50$ MHz [24] that provides satisfactory agreement with the theory.

This standing-wave feature may be observed at comparatively weak drive fields $\Omega\gtrsim\Gamma_{ml}\sim 0.1\Gamma_{mn}$. Note that at $\Gamma_{ml}\ll\Gamma_{mn}$, the splitting should be apparent even earlier than power broadening of the EIT peak, which becomes noticeable at $\Omega\gtrsim\Gamma_{mn}$. Under conditions of the performed experiment, the maximum achievable field amplitude $\Omega=100$ MHz turns out between the characteristic values of the relaxation constants $\Gamma_{ml}\simeq 50$ MHz and $\Gamma_{mn}\simeq 300$ MHz, but the splitting is already expressive, according to the applicability condition. At the same time, the perturbation theory is

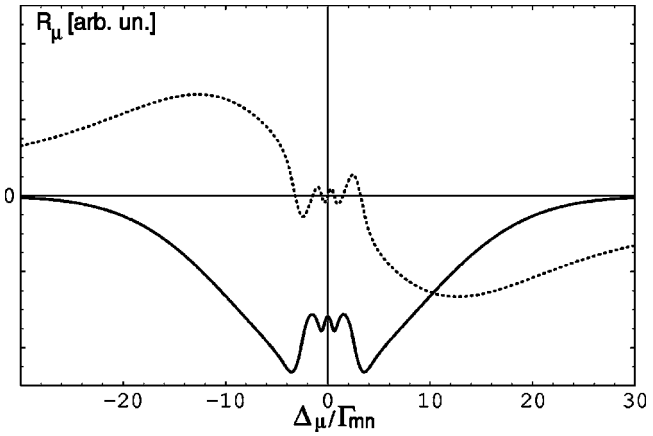

FIG. 5. Doppler broadened absorption contour $-\text{Im}R_\mu$ (solid) and refraction $\text{Re}R_\mu$ (dotted) vs detuning with the same parameters as Fig. 4, but higher intensity $\Omega/\Gamma_{mn}=2$.

still valid at these conditions, and relative amplitude of the EIT peak as well as that for the new resonance remain small enough compared to the Doppler-broadened absorption profile.

We have proved a principle possibility to form different spectral structures within a transparency window by use of standing-wave drive which are relatively narrow: at least two times narrower compared to the window width. Further developments could be concentrated on achievement of extremely narrow structures by this technique that may provide very steep dispersion at high transmission. For this purpose one should increase the amplitude of the drive field Ω significantly. Absorption and dispersion spectra calculated for our (not optimal) relaxation constants at the amplitude five times higher than in the experiment are shown in Fig. 5 together with the absorption background. The transmission peak on the Doppler-broadened absorption contour becomes high and split that results in oscillations of the dispersion with steep slope at the line center, several times steeper compared to usual EIT window. By use of probe transitions with smaller Γ_{ml} (e.g., with ground state involved) one can obtain narrower structures in absolute scale. Note that the effect is also observable for anti-Stokes probe too, namely, in the range $k \leqslant k_{\mu} \leqslant 2k$.

The authors are grateful to S.G. Rautian and A.M. Shalagin for helpful discussions and acknowledge the excellent technical assistance by S.I. Kablukov in the creation of the setup. The work was granted by the RFBR (Project No. 02-02-39025-GFEN) and by a governmental program of support of leading research groups in Russia.

[1] S.E. Harris, Physics Today **50**(7), 36 (1997).
[2] J.P. Marangos, J. Mod. Opt. **45**, 471 (1998).
[3] S.E. Harris, J.E. Field, and A. Imamoğlu, Phys. Rev. Lett. **64**, 1107 (1990).
[4] A.S. Zibrov, M.D. Lukin, D.E. Nikonov, L. Hollberg, M.O. Scully, V.L. Velichansky, and H.G. Robinson, Phys. Rev. Lett. **75**, 1499 (1995).
[5] J.Y. Gao, S.H. Yang, D. Wang, X.Z. Guo, K.X. Chen, Y. Jiang, and B. Zhao, Phys. Rev. A **61**, 023401 (1999).
[6] L.V. Hau, S.E. Harris, Z. Dutton, and C.H. Behroozi, Nature (London) **397**, 594 (1999).
[7] C. Liu, Z. Dutton, C.H. Behroozi, and L.V. Hau, Nature (London) **409**, 490 (2001).
[8] A.V. Turukhin, V.S. Sudarshanam, M.S. Shahriar, J.A. Musser, B.S. Ham, and P.R. Hemmer, Phys. Rev. Lett. **88**, 023602 (2002).
[9] C.Y. Ye and A.S. Zibrov, Phys. Rev. A **65**, 023806 (2002).
[10] M.M. Kash, V.A. Sautenkov, A.S. Zibrov, L. Hollberg, G.R. Welch, M.D. Lukin, Y. Rostovtsev, E.S. Fry, and M.O. Scully, Phys. Rev. Lett. **82**, 5229 (1999).
[11] S.G. Rautian and I.I. Sobel'man, Zh. Éksp. Teor. Fiz. **44**, 934 (1963) [Sov. Phys. JETP **17**, 635 (1963)].
[12] S. Stenholm and W.E. Lamb, Phys. Rev. **181**, 618 (1969).
[13] S. Haroche and F. Hartmann, Phys. Rev. A **6**, 1280 (1972).
[14] B.J. Feldman and M.S. Feld, Phys. Rev. A **5**, 899 (1972).
[15] R. Corbalan, A.N. Pisarchik, V.N. Chizhevsky, and R. Vilaseca, Opt. Commun. **133**, 225 (1997).
[16] F. Silva, J. Mompart, V. Ahufinger, and R. Corbalan, Phys. Rev. A **64**, 033802 (2001).
[17] M.J. Werner and A. Imamoglu, Phys. Rev. A **61**, 011801 (2000).
[18] C.L. Bentley, Jr., J. Liu, and Y. Liao, Phys. Rev. A **61**, 023811 (2000).
[19] S.A. Babin, S.I. Kablukov, S.V. Khorev, E.V. Podivilov, V.V. Potapov, D.A. Shapiro, and M.G. Stepanov, Phys. Rev. A **63**, 063804 (2001).
[20] S.M. Kobtsev, A.V. Korablev, S.V. Kukarin, and V.B. Sorokin, in *Control of Laser Beam Characteristics and Nonlinear Methods for Wavefront Control, Laser Optics 2000, St. Petersburg, 2000*, edited by L.N. Soms and V.E. Sherstobitov (SPIE, Bellingham, WA, 2001), Vol. 4353, pp. 189–193.
[21] G. Stephan and M. Trümper, Phys. Rev. A **30**, 1925 (1984).
[22] S. Stenholm, Phys. Rep. **43**, 151 (1978).
[23] A.K. Popov, *Introduction to Nonlinear Spectroscopy* (Nauka, Novosibirsk, 1983).
[24] S.A. Babin and D.A. Shapiro, Phys. Rep. **241**, 119 (1994).